PHYSICAL REVIEW C **91**, 044318 (2015)

Pygmy resonances and radiative nucleon captures for stellar nucleosynthesis

N. Tsoneva,[1,2] S. Goriely,[3] H. Lenske,[1] and R. Schwengner[4]
[1]*Institut für Theoretische Physik, Universität Gießen, Heinrich-Buff-Ring 16, D-35392 Gießen, Germany*
[2]*Institute for Nuclear Research and Nuclear Energy, 1784 Sofia, Bulgaria*
[3]*Institut d'Astronomie et d'Astrophysique, Université Libre de Bruxelles, Campus de la Plaine, CP 226, 1050 Brussels, Belgium*
[4]*Helmholtz-Zentrum Dresden-Rossendorf, 01328 Dresden, Germany*

(Received 27 February 2015; revised manuscript received 2 April 2015; published 20 April 2015)

The impact of low-energy multipole excitations and pygmy resonances on radiative neutron and proton-capture cross sections in nuclei close to the β-stability line is investigated. For this purpose, a microscopic theoretical approach based on self-consistent density functional theory and quasiparticle-random-phase-approximation formalism extended with multiphonon degrees of freedom is implemented in a statistical reaction model. The advantage of the method is the microscopic nuclear structure input for unified description of low-energy multiphonon excitations and pygmy and giant resonances. This is found to be important for the understanding of the fine structure and dynamics of the nuclear response function at low energies, which strongly influences nuclear reaction rates of astrophysical relevance. Calculations of the radiative capture cross sections of the reactions $^{85}\mathrm{Kr}(n,\gamma)^{86}\mathrm{Kr}$, $^{87}\mathrm{Sr}(n,\gamma)^{88}\mathrm{Sr}$, and $^{89}\mathrm{Y}(p,\gamma)^{90}\mathrm{Zr}$ are discussed in comparison with experimental data. For the reactions $^{89}\mathrm{Zr}(n,\gamma)^{90}\mathrm{Zr}$ and $^{91}\mathrm{Mo}(n,\gamma)^{92}\mathrm{Mo}$ theoretical predictions of the reaction cross sections are made.

DOI: 10.1103/PhysRevC.91.044318 PACS number(s): 21.60.Jz, 24.60.Dr, 25.40.Lw, 27.50.+e

I. INTRODUCTION

The majority of the naturally existing chemical elements in the universe are produced in stars in various nuclear reactions [1–3]. Among the different nuclear processes, the radiative neutron-capture plays a fundamental role because it is believed to be responsible for the formation of the vast majority of the elements heavier than Fe. Depending on the neutron densities N_n invoked, one can distinguish two types of neutron-capture processes, namely, the slow (s) neutron-capture process, which is a low-density process with $N_n \simeq 10^8\ \mathrm{cm}^{-3}$, and the rapid (r) neutron-capture process, at much higher densities, with $N_n \geqslant 10^{20}\ \mathrm{cm}^{-3}$.

With its relatively low neutron density, the s process operates in nuclear-mass regions situated within the valley of β stability (for a review, see [4]). The short-lived radioactive isotopes produced by neutron captures undergo β decay rather than a subsequent neutron capture. However, the s process might also reach longer-lived radioactive nuclei for which the time scales against neutron capture and β decay are comparable. Such nuclei are known as "branching-point" nuclei of the s process and are of particular interest because they can provide information on the neutron flux and temperature at the s-process site [4]. A typical case is the nucleus ^{85}Kr. Recently, the $^{85}\mathrm{Kr}(n,\gamma)^{86}\mathrm{Kr}$ reaction rate was reexamined experimentally and theoretically [5] by large-scale quasiparticle-phonon-model (QPM) calculations [6], resulting in a very satisfactory agreement between data and theory. The new value of the Maxwellian-averaged neutron-capture cross section was found to be about 50% higher than the previous estimates of Ref. [7].

The accuracy was improved considerably by reducing the total error to 50% of the values obtained in previous evaluations [5].

The r process is believed to proceed in explosive stellar environments producing neutron-rich nuclei well beyond the β-stability valley and consequently giving rise to the formation of heavy exotic nuclear systems (for a review, see Ref. [8]). The r-process nucleosynthesis is responsible for about half of the elements heavier than iron, but its astrophysical site remains unidentified. For both s and r processes, the corresponding neutron-capture cross sections are commonly evaluated in the framework of the Hauser-Feshbach (HF) statistical model, which is based on the fundamental assumption of a compound nucleus (CN) in thermodynamical equilibrium [9,10]. In this approach, the Maxwellian-averaged (n,γ) rates at energies relevant to these processes are strongly dependent on the low-energy part of the nuclear dipole response function [11].

In addition to these neutron-capture processes, there is also a certain group of proton-rich nuclei heavier than iron which are located at the neutron-deficient side of the β-stability valley and are not accessible by neutron captures. Those nuclei are known as p-process nuclei. Even though the nature of the p process is not completely understood, the most favored explanation is that it proceeds via a sequence of photodisintegrations of stable preexisting s and r nuclides [12]. Radiative proton captures could also potentially contribute to the production of the lightest p nuclei. Also in this case, the reactions of astrophysical interest strongly depend on the low-energy part of the electromagnetic strength function. When dealing with experimentally inaccessible nuclei, reliable microscopic calculations become of prime interest for such astrophysics applications, as discussed in Refs. [8,12].

Recently, much attention has been given to the understanding of a low-energy electromagnetic excitation mode called pygmy dipole resonance (PDR) [13]. The PDR appears as an additional dipole strength component around the neutron threshold sitting on top of the low-energy tail of the giant dipole resonance (GDR) classically represented by a Lorentzian shape [14–16]. This phenomenon is found to be a common feature in stable and unstable neutron-rich nuclei. The PDR states are understood as oscillations of weakly bound neutrons from the Fermi surface with respect to the isospin-symmetric nuclear core [17,18]. From systematic studies of nuclear isotonic and isotopic chains, a correlation of total PDR strengths and nuclear skin thickness was found [15,16,18–20]. Furthermore, the detailed analysis of pygmy dipole strengths in $N = 50$ isotones [16] shows that standard strength functions based on Lorentz curves currently used for the calculation of cross sections in statistical reaction model codes do not describe the dipole strength distribution below the (γ,n) threshold correctly and need to be improved. Another interesting aspect of the low-energy excitations and in particular of the PDR is that they incorporate interactions resulting from multiparticle-multihole couplings and core polarization effects induced by the GDR.

Obviously, an approach like the quasiparticle-random-phase-approximation (QRPA) [21], considering only coherent superpositions of two-quasiparticle excitations, is not sufficient to account for the complexity of phenomena in the PDR region. Rather, an extended approach is required which explicitly accounts for the interactions among multi-quasiparticle configurations. Presently, the three-phonon QPM approach [22] is a successful method allowing for a unified description of low-energy single- and multiple-phonon states and the GDR. Such a unified treatment is exactly what is required to separate the multiphonon and the genuine PDR strengths in a meaningful way [18]. An important advantage of the QPM in comparison with other methods incorporating quasiparticle-phonon coupling [23–26] is the use of sufficiently large configuration spaces. They are the most important prerequisite for quantitative descriptions and predictions of nuclear data. Nuclear shell-model calculations are typically limited to one or a few valence orbits, especially in the mass regions of interest for astrophysics.

Recent theoretical studies [11,27–29] indicate that the existence of PDR might have a large impact on neutron-capture reaction cross sections contributing to the nucleosynthesis. However, those investigations were based mostly on QRPA strength distributions which needed to be broadened and renormalized on GDR data to account for missing effects such as the phonon coupling [27,28]. Recently, calculations of neutron-capture cross sections on the basis of γ-ray strength functions estimated beyond QRPA, including nonrelativistic [23] and relativistic [25] approaches, were performed in neutron-rich Sn and Ni isotopes. In these studies the importance of the quasiparticle-phonon coupling for low-energy dipole strength functions is highlighted. The precise knowledge and proper description of the complex structure of the low-energy excited states and PDR is known to be of prime importance for the calculation of nuclear reaction rates of astrophysical importance. In this respect, details of the fine and gross structure and dynamics of the nuclear response function around the neutron threshold should be taken into account.

The aim of the present work is to reveal the predictive power of an advanced microscopic nuclear structure model based on the self-consistent energy-density functional (EDF) theory and QPM in the studies of radiative neutron- and proton-capture cross sections in $N = 50$ nuclei. For comparison, we have performed two different kinds of QRPA calculations with respect to the nuclear mean-field and residual interactions used in the calculations of the nuclear excited states. The first method includes nuclear mean field determined by EDF formalism linked to self-consistent Skyrme (SLy4) Hartree Fock Bogoliubov (HFB) calculations and the separable residual interactions of the QPM, which are explained in Secs. II and III B and Refs. [6,18]. The second approach, is based on a self-consistent HFB + QRPA model which incorporates BSk7 Skyrme force. In this case, the mean field and the residual interaction are derived consistently from the Skyrme (BSk7) EDF, as discussed in Sec. III B and in Refs. [27,28,30]. The HFB + QRPA calculation with the BSk7 force has been widely tested on experimental radiative neutron-capture and photodisintegration data, as well as used for nucleosynthesis applications [8].

Furthermore, the newly derived $E1$ strengths in $N = 50$ isotones are used to estimate reaction cross sections within the formalism described in Sec. III. More specifically, in Sec. IV, the $E1$ strengths and neutron-capture reactions ^{85}Kr$(n,\gamma)^{86}$Kr, ^{87}Sr$(n,\gamma)^{88}$Sr, ^{89}Zr$(n,\gamma)^{90}$Zr, and ^{91}Mo$(n,\gamma)^{92}$Mo are studied with various predictions of the γ-strength function and compared with available experimental data. For all these cases, the role of the PDR is examined and discussed in detail. For the ^{89}Zr and ^{91}Mo neutron-capture cases, which are hardly accessible experimentally because of the short lifetime of the targets, the radiative capture cross sections of the reactions are theoretically predicted. Finally, the proton radiative capture reaction ^{89}Y$(p,\gamma)^{90}$Zr for which experimental data exist is also studied to test the newly derived strength functions. Conclusions are drawn in Sec. V.

II. THE THEORETICAL APPROACH

Microscopic model of nuclear ground and excited states

A successful description of the low-energy γ-ray strength, and more particularly of the PDR, could be achieved in a microscopic theoretical approach which incorporates the EDF theory and the three-phonon QPM [18,20]. Recently the method was implemented in the description of the structure of nuclear electric and magnetic excitations in the PDR region [31,32].

The model Hamiltonian is given by

$$H = H_{\mathrm{MF}} + H_{\mathrm{res}}, \tag{2.1}$$

where H_{MF} is a mean-field part and H_{res} stands for the residual interaction. The mean-field part defined as

$$H_{\mathrm{MF}} = H_{\mathrm{sp}} + H_{\mathrm{pair}} \tag{2.2}$$

is treated by self-consistent HFB theory [33]. The term H_{sp} defines the single-particle properties of quasiparticles in a static and spherically symmetric mean field, which is generated self-consistently by their mutual interactions, including a monopole pairing interaction H_{pair} in the particle-particle channel. The pure HFB picture is, in fact, extended beyond mean field by dynamical self-energies, hence incorporating a more detailed spectral description of nuclear spectra. That goal is achieved in practice by taking advantage of the Kohn-Sham theorem [34,35] of the EDF theory and applying fully microscopic HFB potentials and pairing fields as input.

TABLE I. HFB results obtained with the phenomenological EDF of the total binding energy, mass, and charge radii and the related skin thickness δr defined with Eq. (2.3) are compared to measured binding energies [36].

Nucleus	$B(A)/A_{(\mathrm{EDF})}$ (MeV)	$B(A)/A_{(\mathrm{exp})}$ (MeV)	$\sqrt{r_p^2}$ (fm)	$\sqrt{r_n^2}$ (fm)	δr (fm)
^{86}Kr	−8.755	−8.712	4.131	4.264	0.133
^{88}Sr	−8.766	−8.733	4.185	4.291	0.106
^{90}Zr	−8.696	−8.710	4.229	4.303	0.074
^{92}Mo	−8.596	−8.658	4.269	4.325	0.056

Further, a second step variation procedure is performed with scaled auxiliary potentials and pairing fields readjusted in a self-consistent manner such that nuclear binding energies and other ground-state properties like the charge radii and the neutron skin thickness given by the differences of proton and neutron root-mean-square radii,

$$\delta r = \sqrt{\langle r^2\rangle_n} - \sqrt{\langle r^2\rangle_p}, \tag{2.3}$$

reproduce the results obtained from Skyrme SLy4 HFB calculations [18] and the available experimental data of [36] within uncertainties below 1%. The total binding energy per nucleon as obtained by the EDF as well as the mass, the charge radii, and the related skin thicknesses in $N = 50$ isotones are compared with the data of Ref. [36] in Table I.

A reliable description of ground-state properties is of genuine importance for extrapolations of QRPA and QPM calculations into unknown mass regions. Calculations of ground-state neutron and proton densities for $Z = 50$ and $N = 50, 82$ nuclei are shown in Refs. [16,18]. Of special importance for these investigations are the nuclear surface regions, where the formation of a skin takes place. A common observation found in the investigated isotopic and isotonic chains of nuclei is that the thickness of the neutron skin is related to the neutron-to-proton ratio N/Z, which is demonstrated also in Table I for the $N = 50$ isotones. An interesting example as well is the tin isotopic chain. In this case, in the Sn nuclei with $A \geqslant 106$ the neutron ground-state distributions at the nuclear surface begin to extend beyond the proton ones and the effect continues to increase with the neutron excess and beyond of ^{132}Sn. Thus, these nuclei have a neutron skin. The situation reverses in $^{100-102}$Sn, where a tiny proton skin appears [18]. The presence of a proton skin can affect the structure of low-energy excitations related to PDR [29]. Similar effects were also found in our recent theoretical investigations of higher-order multipole pygmy resonance, namely the pygmy quadrupole resonance which has been for the first time predicted in Sn nuclei [37].

The nuclear excited states are calculated with a residual interaction which is based on the QPM formalism [6],

$$H_{\mathrm{res}} = H_{\mathrm{M}}^{\mathrm{ph}} + H_{\mathrm{SM}}^{\mathrm{ph}} + H_{\mathrm{M}}^{\mathrm{pp}}, \tag{2.4}$$

where effective interactions are implemented to account for the interaction between the quasiparticles. The terms $H_{\mathrm{M}}^{\mathrm{ph}}$, $H_{\mathrm{SM}}^{\mathrm{ph}}$, and $H_{\mathrm{M}}^{\mathrm{pp}}$ are taken as a sum of isoscalar and isovector separable multipole and spin-multipole interactions in the particle-hole and multipole pairing interaction in the particle-particle channels, respectively [6]. The model parameters are fixed empirically in such a way that the properties of the lowest-lying collective states and giant resonances are described accurately [38].

The nuclear excitations are expressed in terms of QRPA phonons which are defined [6] with the equation

$$Q_{\lambda\mu i}^{+} = \frac{1}{2}\sum_{jj'}\left[\psi_{jj'}^{\lambda i}A_{\lambda\mu}^{+}(jj') - \varphi_{jj'}^{\lambda i}\widetilde{A}_{\lambda\mu}(jj')\right], \tag{2.5}$$

where $j \equiv (nljm\tau)$ is a single-particle proton or neutron state; $A_{\lambda\mu}^{+}$ and $\widetilde{A}_{\lambda\mu}$ are time-forward and time-backward operators, coupling two-quasiparticle creation or annihilation operators to a total angular momentum λ with projection μ by means of the Clebsch-Gordan coefficients $C_{jmj'm'}^{\lambda\mu} = \langle jmj'm'|\lambda\mu\rangle$. The excitation energies of the phonons and the time-forward and time-backward amplitudes $\psi_{j_1j_2}^{\lambda i}$ and $\varphi_{j_1j_2}^{\lambda i}$ in Eq. (2.5) are determined by solving QRPA equations [6].

The phonon operators satisfy the commutation relation:

$$\begin{aligned}[Q_{\lambda\mu i}, Q_{\lambda'\mu'i'}^{+}] &= \frac{\delta_{\lambda,\lambda'}\delta_{\mu,\mu'}\delta_{i,i'}}{2}\sum_{jj'}\left[\psi_{jj'}^{\lambda i}\psi_{jj'}^{\lambda i'} - \varphi_{jj'}^{\lambda i}\varphi_{jj'}^{\lambda i'}\right]\\ &\quad - \sum_{jj'j_2}\sum_{mm'm_2}\left\{\psi_{j'j_2}^{\lambda i}\psi_{jj_2}^{\lambda' i'}C_{j'm'j_2m_2}^{\lambda\mu}C_{jmj_2m_2}^{\lambda'\mu'}\right.\\ &\quad \left. - (-)^{\lambda+\lambda'+\mu+\mu'}\varphi_{jj_2}^{\lambda i}\varphi_{j'j_2}^{\lambda' i'}C_{jmj_2m_2}^{\lambda-\mu}C_{j'm'j_2m_2}^{\lambda'-\mu'}\right\}\\ &\quad \times \alpha_{jm}^{+}\alpha_{j'm'}.\end{aligned} \tag{2.6}$$

The first term of the commutator (2.6) corresponds to the QRPA, which is also called a "quasiboson" approximation as far the QRPA phonons are associated with pure boson states [39]. However, to satisfy the Pauli principle one must take into account the internal fermionic structure of the phonons which is achieved by the second term of the commutator (2.6).

Furthermore, the QPM provides a microscopic approach to multiconfiguration mixing [6]. In our approach, the wave function of an excited state consists of one-, two-, and three-phonon configurations [22],

$$\begin{aligned}\Psi_\nu(JM) = \Bigg\{&\sum_i R_i(J\nu)Q_{JMi}^{+} + \sum_{\substack{\lambda_1 i_1\\ \lambda_2 i_2}} P_{\lambda_2 i_2}^{\lambda_1 i_1}(J\nu)\\ &\times \left[Q_{\lambda_1\mu_1 i_1}^{+} \times Q_{\lambda_2\mu_2 i_2}^{+}\right]_{JM} + \sum_{\substack{\lambda_1 i_1\lambda_2 i_2\\ \lambda_3 i_3 I}} T_{\lambda_3 i_3}^{\lambda_1 i_1\lambda_2 i_2 I}(J\nu)\\ &\times \left(\left[Q_{\lambda_1\mu_1 i_1}^{+} \otimes Q_{\lambda_2\mu_2 i_2}^{+}\right]_{IK} \otimes Q_{\lambda_3\mu_3 i_3}^{+}\right)_{JM}\Bigg\}\Psi_0,\end{aligned} \tag{2.7}$$

where R, P, and T are unknown amplitudes to be obtained from the equation of motion [6], ν labels the number of the excited states, and Ψ_0 is the phonon vacuum state.

The electromagnetic transitions are described by transition operators accounting for the internal fermionic structure of the phonons [39]. The method allows for sufficiently large configuration spaces such that a unified description of low-energy single- and multiple-phonon states and the GDR is feasible. Such a unified treatment is exactly what is required to separate the multiphonon and the genuine PDR 1^- strengths in a meaningful way.

The character of a nuclear excitation could be examined by considering the spatial structure of the transition. This is accomplished by analyzing the one-body transition densities $\delta\rho(r)$ which are the nondiagonal elements of the nuclear one-body density matrix. Physically, $\delta\rho(r)$ corresponds to the density fluctuations induced by the action of a one-body operator associated with external electromagnetic field on the nucleus. Hence, the transition densities are directly related to the nuclear response functions and by analyzing their spatial pattern we obtain a very detailed picture of, e.g., the radial distribution and localization of the excitation process. The particular usefulness of such an analysis for PDR states was pointed out in Refs. [16,18].

III. NUCLEAR INGREDIENTS FOR TALYS CALCULATIONS OF NUCLEON-NUCLEUS-CAPTURE CROSS SECTIONS

Nuclear-reaction calculations consider, as input, nuclear ingredients which are taken as much as possible from experiment [9,10,40]. However, the significance of modern microscopic approaches increases extremely, in particular when dealing with short-lived isotopes and exotic nuclei which could not be reached experimentally. Such microscopic nuclear structure investigations are also more reliable than predictions derived from phenomenological approaches as described in Refs. [10,40] and can be used nowadays directly as an input in nuclear reaction codes.

The present cross-section calculations are performed using the updated version of the TALYS code [9], a statistical-model software for the simulation of nuclear reactions. The code provides a comprehensive description of all known reaction channels and observables and, in particular, takes into account all different types of nuclear processes related to direct, preequilibrium, and compound mechanisms [10]. The model is able to estimate total and partial reaction probabilities accounting for the competition between the various open channels. For that purpose, many state-of-the-art nuclear models which cover completely reaction mechanisms encountered in light-particle-induced nuclear reactions are included, as presented in Ref. [9]. Whenever available, experimental information on nuclear masses, deformation, and spectra of low-lying states is considered. In particular, a major source of experimental information comes from the RIPL-3 database [40]. When no experimental data exists, TALYS is supported by various local and global input models which account for the nuclear structure properties, such as ground-state energies, deformations, nuclear densities, shell corrections, nuclear-level densities, etc., but also interaction properties for the optical potentials and electromagnetic response functions.

As mentioned in the Introduction, the reaction rates of astrophysical interest are commonly evaluated in the framework of the HF statistical model, the formation of a CN being justified by the large nuclear level density (NLD) in the CN at the projectile incident energy and consequently ensuring an average statistical continuum superposition of available resonances. For medium- and heavy-mass nuclei lying within the valley of stability, including the $N \simeq 50$ nuclei studied in the present work, the resonant capture at low energies of astrophysical interest (i.e., typically below a few MeV) is therefore known to be the dominant reaction mechanism, whereas the direct and preequilibrium contributions appear to be negligible [10].

The fundamental concept of the HF statistical nuclear reaction model is based on the formation of the CN, which consequently decays, obeying the energy E, momentum J, and parity π conservation laws, to different exit channels [9,10,41]. Therefore, for a given combination of the conserved quantities, the probability of a specific reaction is a product of the probability for formation of the CN in the entrance channel and the probability for its decay into the exit channel. These probabilities are known as transmission coefficients T and are estimated as a sum over all partial contributions T^x from excited states x in the CN with experimentally known energy, spin, and parity.

At excitation energies for which the required data are not available, this sum transforms into an integral over a NLD, so that

$$T(J^\pi) = \sum_{x=0}^{\omega} T^x(J^\pi) + \int_{E_\omega}^{E_c} \int_{J_x\pi_x} T^x(E_x, J^\pi) \times \rho(E_x, J_x, \pi_x)\, dE_x\, d\pi_x\, dJ_x, \tag{3.1}$$

where E_c is the excitation energy of the CN formed after the neutron capture, E_ω is the energy of the highest experimentally known excited state ω, and $\rho(E_x, J_x, \pi_x)$ is the density per unit energy interval states with spin J_x and parity π_x at the excitation energy E_x.

As far as the electromagnetic channel is concerned, the $E1$ mode is known to dominate and the excitation of multipolarities larger than 1 not to play a major role, at least for medium and heavy targets. For the dominant electric dipole γ emission, similarly to Eq. (3.1), the continuum contribution to the transmission coefficient can be evaluated with the integral relation

$$T_\gamma \approx \int_{E_\omega}^{E_c} \rho(E_x, 1, -) T_{E1}(E_c - E_x)\, dE_x, \tag{3.2}$$

where T_{E1} is the $E1$ transmission coefficient for the electromagnetic deexcitation from the initial nuclear state of energy E_c to the final state of energy E_x; $\rho(E_x, 1, -)$ is the level density of the final nucleus state corresponding to an electric dipole transition, i.e., $|J_c - J_x| = 1$ and $\pi_c \pi_x = -1$. The energy of the emitted photon E_γ is given by the relation $E_\gamma = E_c - E_x$.

The γ transmission coefficient [Eq. (3.2)] is related to the downward deexcitation γ-ray strength function $f_{E1}^{\downarrow}$ by $T_\gamma(E1) = 2\pi E_\gamma^3 f_{E1}^{\downarrow}$. The $f_{E1}^{\downarrow}$ is traditionally associated with the photoabsorption strength on the basis of the Brink hypothesis [42], i.e., $f_{E1}^{\downarrow} = f_{E1}^{\uparrow}$, which, in turn, is related to the photoabsorption cross section by $\sigma_{\text{abs}}(E_\gamma) = 3(\pi\hbar c)^2 E_\gamma f_{E1}^{\uparrow}(E_\gamma)$. Note that the contributions to the electromagnetic transmission coefficient stemming from the $M1$, $E2$, $M2$, ... transitions are also taken into account and their respective strengths estimated following the recommendation described in Ref. [40].

Consequently, the precise knowledge of level densities and dipole response functions is of crucial importance for the study of nuclear-reaction cross sections. Note that the optical potential does not affect significantly the prediction of the radiative neutron-capture cross section at energies below a few MeV because the neutron transmission coefficient through the strong interaction dominates over the electromagnetic one [10]. This property might, however, not hold for very exotic neutron-rich nuclei, as shown in Ref. [43]. In the present study, the nucleon optical potential of Ref. [44] is used. More details on the adopted NLD and $E1$ models are given in Sec. III A.

A. Nuclear-level density and discrete-level scheme

The NLD, as discussed above, is an important ingredient for our investigations of radiative nucleon-capture cross sections in $N = 50$ isotones. However, it is well known that experimental data about the spectrum of excited states exist mainly for stable nuclei and it is generally restricted to certain energy ranges and far from being complete. Even more for most nuclei, outside the stability region, experimental levels are not available. In this situation, as a common theoretical procedure a continuum level spectrum determined from a NLD model is used. Many studies have been devoted to the evaluation of the NLD. The so-called partition function method is by far the most widely used technique for calculating level densities, particularly in view of its ability to provide simple analytical formulas. In its simplest form, the NLD is evaluated for a gas of noninteracting fermions confined to the nuclear volume and having equally spaced energy levels. Such a model corresponds to the zeroth-order approximation of a Fermi gas model and leads to very simple analytical expressions for the NLD. In an attempt to reproduce the experimental data, various phenomenological modifications to such an analytical formulation of have been suggested, in particular to allow for shell, pairing, and collective effects. This led first to the constant-temperature formula, then to the shifted Fermi gas model, and later to the popular backshifted Fermi gas model [40,45–49].

However, drastic approximations are usually made in deriving such analytical NLD formulas and their shortcomings in matching experimental data are overcome by empirical parameter adjustments. Several of the approximations used to obtain the NLD expressions in an analytical form can be avoided by quantitatively taking into account the discrete structure of the single-particle spectra associated with realistic effective potentials. This approach leads to the so-called microscopic statistical model (e.g., [50,51]), as well as other various microscopic models, including, for example, the combinatorial [52–54], spectral distribution [55], Monte Carlo [56], and quantum Monte Carlo approaches, including correlations beyond the mean-field approximation [57,58]. In the present study, the default model of NLD is the HFB plus combinatorial model of Ref. [53].

B. Nuclear response function

Dipole photoabsorption cross sections obtained from the EDF + QRPA, EDF + three-phonon QPM (based on SLy4

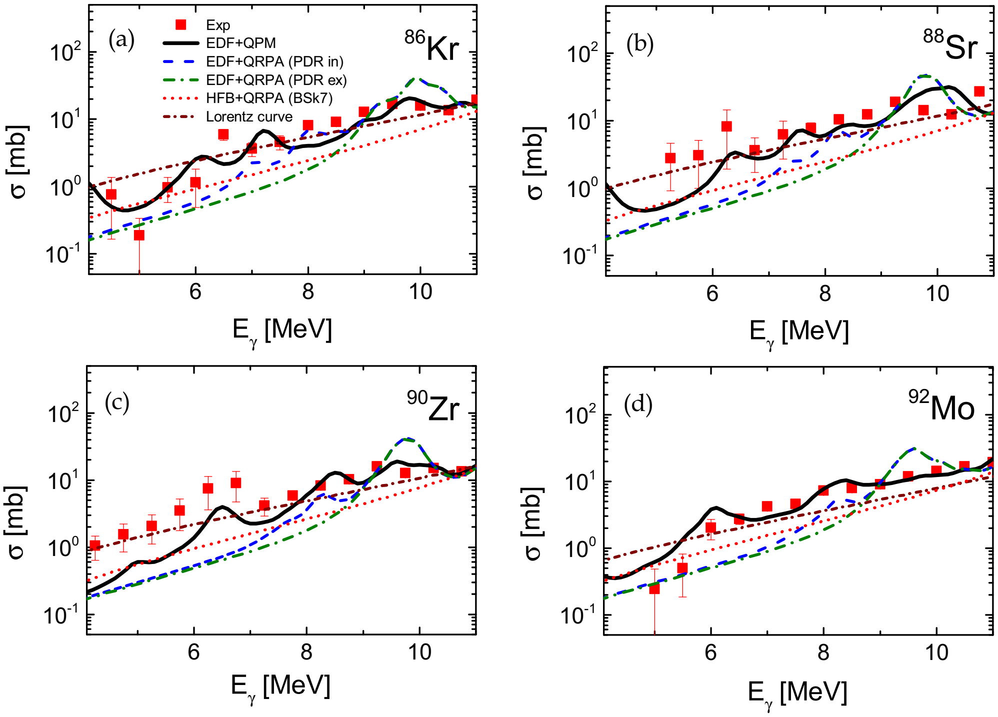

FIG. 1. (Color online) Systematic EDF + QRPA including PDR (blue dashed line), EDF + QRPA excluding PDR (green long-dash-dotted line), three-phonon EDF + QPM (black solid line), HFB + QRPA calculation based on the BSk7 force (red dotted line), and standard Lorentz curves (brown short-dash-dotted line) with parameter sets from Table II calculations of dipole photoabsorption cross section below the neutron threshold of (a) ^{86}Kr, (b) ^{88}Sr, (c) ^{90}Zr, (d) ^{92}Mo ($N = 50$ nuclei) in comparison with experimental data [16].

TABLE II. RIPL-2 recommended parameters for the standard Lorentzian curve (SLO) used to approximate the shape of the GDR, i.e., the peak energy $E_{\mathrm{GDR}}^{\max}$, the peak cross section $\sigma_{\mathrm{GDR}}^{\max}$, and the full width at half maximum Γ_{GDR}.

Nucleus	$E_{\mathrm{GDR}}^{\max}$ (MeV)	$\sigma_{\mathrm{GDR}}^{\max}$ (mb)	Γ_{GDR} (MeV)
^{86}Kr	17.10	206	4.70
^{88}Sr	16.84	206	4.50
^{90}Zr	16.74	211	4.16
^{92}Mo	16.82	162	4.14

force), and HFB + QRPA (based on BSk7 Skyrme force) are presented in Fig. 1. The theoretical results are compared to experimental data from Ref. [16].

The EDF + QRPA and EDF + QPM calculations use a separable residual interaction which is described in Sec. II and in Ref. [6]. Here the determination of the model parameters follows closely the prescription given in Refs. [18,38] and it is in agreement with our previous studies of $N = 50$ isotones reported in Ref. [16]. Thus, the dipole isoscalar coupling constant of the particle-hole channel is obtained by projecting the spurious 1^- state to zero excitation energy and the dipole isovector coupling constant of the particle-hole channel is fixed by fitting the experimental energy of the maximum of the GDR, $E_{\mathrm{GDR}}^{\max}$. The experimental values $E_{\mathrm{GDR}}^{\max}$ for $N = 50$ nuclei are given in Table II, where also complete parameter sets of the standard Lorentzian fit extracted from the RIPL-2 database [45] are given. The latter corresponds to an approximate shape of the GDR fitted in the vicinity of the centroid energy. The corresponding Lorentzian curves in $N = 50$ nuclei are shown in Fig. 1.

The HFB plus QRPA calculations based on the BSk7 Skyrme force are described in detail in Refs. [27,28,30]. In addition to the standard QRPA formalism, some phenomenolgical corrections are included to take effects related to deformation and to the damping of the collective motion into account. Such a calculation is based on the BSk7 Skyrme force [59], which has been fitted to essentially all known masses and reproduces the 2355 experimental masses of the atomic mass evaluation [36] with a root-mean-square deviation of only 0.682 MeV. In addition, the HFB + QRPA calculation of the $E1$ strength based on this BSk7 force was shown to reproduce satisfactorily the location and width of the GDR and the average resonance capture data at low energies [28]. This QRPA calculation has been extended to all the 8000 $8 \leqslant Z \leqslant 110$ nuclei lying between the proton and neutron drip lines. The $E1$ strength based on the HFB + QRPA (BSk7) model for the $N = 50$ nuclei are also shown in Fig. 1.

IV. RESULTS AND DISCUSSION

A. The $E1$ strength function

Systematic EDF + QRPA and EDF + QPM calculations of the electric dipole response in different isotopic and isotonic chains of nuclei [15,16,18–20] consistently predict the enhanced $E1$ strength in the energy range below the neutron threshold with respect to the shape of a Lorentz-like strength function used to adjust the GDR. In this paper, we focus on the $N = 50$ isotones presented in Fig. 1 (see also Ref. [16]). A common observation in nuclei with neutron skin is that the total $E1$ QRPA strength associated with the PDR increases with the increase of the isospin asymmetry of the nucleus defined by the N/Z ratio [15,18–20,27,28]. Similar results are also reported by various experiments [13]. Exceptions are recent data on ^{120}Sn, which are in a contradiction with theoretical predictions from [24]. This case should be further examined.

The correlation between the total PDR strength obtained in EDF + QRPA calculations and the neutron skin thickness δr in $N = 50$ isotones is shown in Fig. 2. This correlation is explained as follows. By definition, the QRPA excited states are built only from single p-h contributions to the state vectors [see Eq. (2.5)]. For neutron-rich nuclei, within the QRPA representation, the PDR is formed by a sequence of 1^- excited states, whose structure is dominated by oscillations of weakly bound, almost pure neutron two-quasiparticle configurations. The increase of the total PDR strength towards more neutron-rich nuclei can be related to the increase of the amount of those weakly bound quasiparticle neutron states around the Fermi surface which is directly linked to the decrease of the neutron binding energy and the increase of the absolute value of the difference between proton and neutron Fermi energies, $\Delta_F = \epsilon_p^F - \epsilon_n^F$. The latter is correlated linearly with the neutron skin thickness [13]. That type of correlation is easily derived in a local Fermi-gas approximation where the Fermi energies are given by the square of the local Fermi momenta,

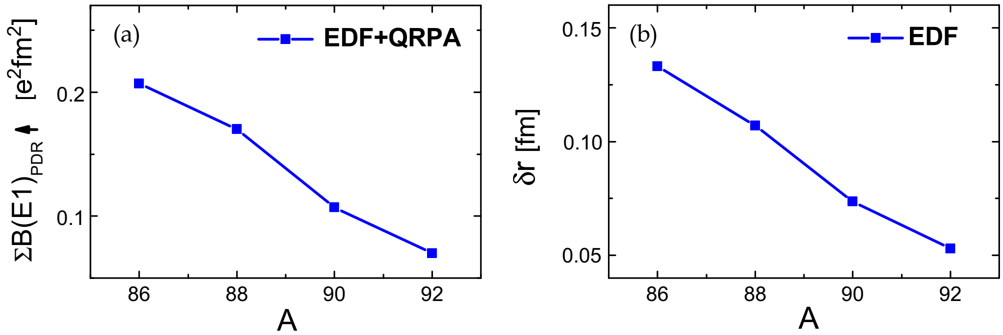

FIG. 2. (Color online) (a) EDF + QRPA calculations of the total $B(E1)_{\mathrm{PDR}}$ strength in stable even-even $N = 50$ nuclei (where the summation is taken in the energy region below $E_\gamma \leqslant 9$ MeV related to PDR [16,18]) as a function of the mass number A. (b) Neutron skin thickness δr as a function of A for the same nuclei.

$k^F_{p,n} \sim \rho^{1/3}_{p,n}$, thus leading to $\Delta_F \sim \rho_p^{2/3} - \rho_n^{2/3}$. Integration over the nuclear volume results in a relation given in leading order by $\Delta_F \sim Z^{2/3}R_p - N^{2/3}R_n$, where $R_{p,n}$ denotes the proton and neutron density radius, respectively. This trend is illustrated with the QRPA calculations in $N = 50$ isotones shown in Fig. 2. The energy region below $E_\gamma \leqslant 9$ MeV is related to the PDR [16,18], whose total strength smoothly decreases with increasing proton number Z.

With increasing excitation energies, the isovector dipole strength increases steadily, following closely the slope of the GDR which in data analyses is assumed to be of Lorentzian shape; see, e.g., [14]. Theoretically, this can be seen in transition densities and state vector structures which manifest an enlarging of the out-of-phase neutron to proton contributions and corresponding energy-weighted sum rules, which is generally associated with the GDR [16,18].

It is clear that the QRPA formalism which uses a model space built of pure two-quasiparticle phonon states and defined by the Eqs. (2.5) and (2.6) is unable to account for correlations of higher multiparticle-multihole correlations and interactions resulting from core polarization effects and GDR. Such contributions are sources of dynamical redistribution of the low-energy dipole transition strength in the nucleus and can strongly affect the gross and fine structure of the nuclear response function. A comparison of EDF + QRPA calculations of dipole photoabsorption cross sections in $N = 50$ isotones obtained in two different cases, when the PDR is included (PDR in) or excluded (PDR ex) by a selection of the QRPA 1^- excited states, is shown in Fig. 1. Our EDF + QRPA (PDR in) findings point out that the PDR has a peak in the dipole photoabsorption cross section at about $E_\gamma = 8$ MeV, which smoothly moves up to higher excitation energy towards ^{92}Mo. More specifically, the EDF + QRPA (PDR in) calculation in ^{86}Kr gives a 56% increase of the total dipole photoabsorption cross section in the PDR energy region compared to the EDF + QRPA (PDR ex) calculations. The effect gradually reduces with the increase of the proton number Z, reaching about 25% in ^{92}Mo.

A comparison between the theoretical results and experimental data is also shown in Fig. 1. It is seen that, in general, the QRPA results underestimate significantly the low-energy data. Furthermore, QRPA calculations, as well as standard Lorentzian approximations, are not able to describe in detail the complex dynamics of the low-energy dipole response function owing to the interference of low-energy excited states, PDR and GDR.

Experimental data can be significantly better explained if the interaction between quasiparticles and phonons [6] is taken into account in the framework of the three-phonon EDF + QPM. A comparison among EDF + QRPA, the three-phonon EDF + QPM, and data is shown in the same Fig. 1. It indicates that in the PDR region the coupling of QRPA PDR and GDR phonons and multiphonon states is very important. The result is a shift of the $E1$ strength to lower energies which can be described in three-phonon QPM formalism also quantitatively [16]. Furthermore, the EDF + QPM calculations have been proven to reproduce the detailed structure of the low-energy multiphonon excitations in our previous studies of $E1$, $E2$, and $M1$ low-energy excitations and giant resonances [31,32,37]. The importance of the precise knowledge of nuclear dipole response functions is further examined in investigations of nuclear-reaction cross sections.

B. Neutron captures

Recently, our EDF + QRPA and three-phonon QPM microscopic strength functions have been implemented into the TALYS reaction code to investigate the ^{85}Kr$(n,\gamma)^{86}$Kr cross sections of astrophysical relevance [5]. It was found that the neutron-capture cross section calculated with the EDF + three-phonon QPM is in very good agreement with experimental data [5], while the EDF + QRPA underestimates the data by about 35%. Here we extend our studies by analyzing systematically the neutron-capture reactions in $N = 50$ isotones for the additional ^{87}Sr$(n,\gamma)^{88}$Sr, ^{89}Zr$(n,\gamma)^{90}$Zr, and ^{91}Mo$(n,\gamma)^{92}$Mo reactions. TALYS calculations are performed using the $E1$ strength functions from EDF + QRPA(SLy4) with (PDR in) and without (PDR ex) including the PDR contribution to investigate its impact on the cross section. The contribution of the pure PDR to radiative capture cross sections for 10–100-keV incident neutrons is estimated to be of the order of ~50% for ^{85}Kr$(n,\gamma)^{86}$Kr, ~22% for ^{87}Sr$(n,\gamma)^{88}$Sr, ~13% for ^{89}Zr$(n,\gamma)^{90}$Zr, and ~10% for ^{91}Mo$(n,\gamma)^{92}$Mo, as shown in Fig. 3.

As far as the QPM predictions are concerned, it can be seen in Fig. 3 that it leads to radiative neutron-capture cross sections higher than the one obtained on the basis of the QRPA strength by a factor of about 2 [or slightly less in the ^{89}Zr$(n,\gamma)^{90}$Zr case]. The higher cross section with the QPM strength is directly related to the enhanced strength stemming from the phonon coupling below the neutron threshold (Fig. 1). It should be remembered that in radiative neutron cross section for incident neutrons with keV energies, the γ energies of relevance are found below the neutron separation energies. To illustrate this fact, we show in Fig. 4 the partial radiative cross section after γ-emission for incident neutrons at an energy $E_n = 100$ keV as a function of the excitation energies E in the CN. These partial cross sections correspond to the four reactions studied in Fig. 3. At the lowest energies E, known discrete excited states are considered, while above the last known level a continuum NLD gives rise to a smooth cross section. To each energy E corresponds the emission of a photon of energy $E_\gamma = S_n + E_n - E$. The corresponding cross section as a function of E_γ is directly linked to the $E1$ transmission coefficient given by Eq. (3.2). Consequently, Fig. 4 illustrates the energy domain in which the $E1$ strength function is of particular relevance to the radiative neutron-capture cross section. This domain is seen to be in the 4–6-MeV range of γ-ray energy or 6–8-MeV excitation energies in the compound system, i.e., significantly lower than the neutron separation energy which for these cases ranges between 10 and 12.6 MeV. Some strong $E1$ deexcitation transitions to low-lying discrete levels are also seen to contribute significantly, in particular in ^{88}Sr and ^{90}Zr.

In the case of the QPM, the major contribution to the ^{85}Kr and ^{87}Sr neutron-capture cross section originates from the strength function around 4-MeV photons. In this energy range of 4–5 MeV, the QPM strength in the CN is found to be

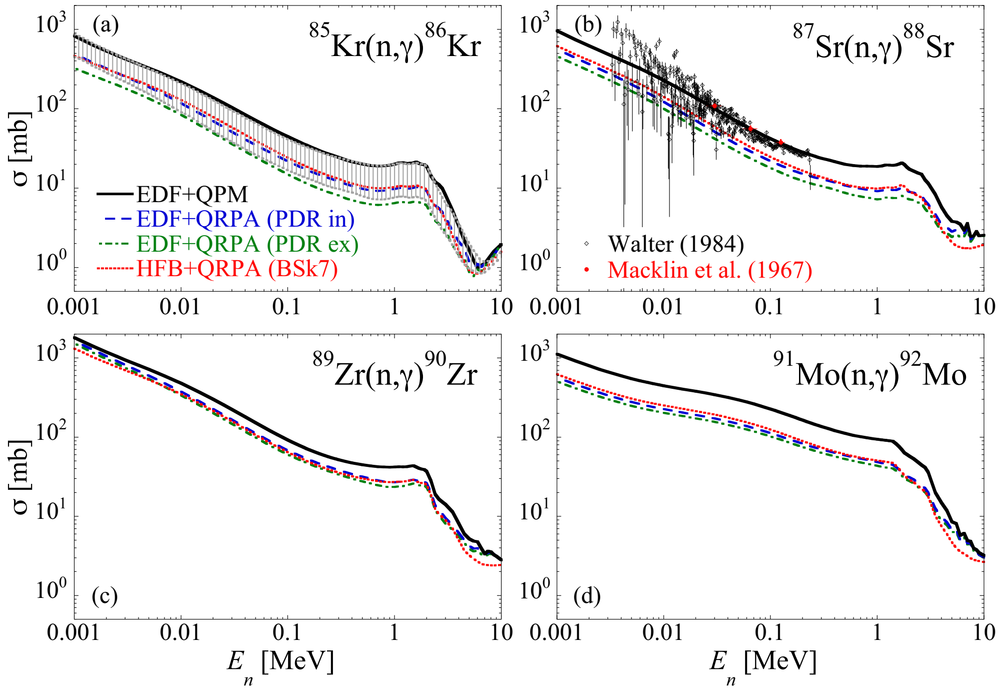

FIG. 3. (Color online) Ground-state neutron-capture cross sections of (a) ^{85}Kr$(n,\gamma)^{86}$Kr, (b) ^{87}Sr$(n,\gamma)^{88}$Sr, (c) ^{89}Zr$(n,\gamma)^{90}$Zr, and (d) ^{91}Mo$(n,\gamma)^{92}$Mo calculated with TALYS using EDF plus three-phonon QPM (black solid line), EDF + QRPA (PDR included) (blue dashed line), EDF + QRPA (PDR excluded) (green dash-dotted line), and HFB + QRPA (BSk7) (red dotted line) strength functions. For ^{85}Kr$(n,\gamma)^{86}$Kr, the hatched area corresponds to the cross section determined with the experimental strength as derived in Ref. [5]. For ^{87}Sr$(n,\gamma)^{88}$Sr, TALYS cross sections are compared with experimental data [60,61].

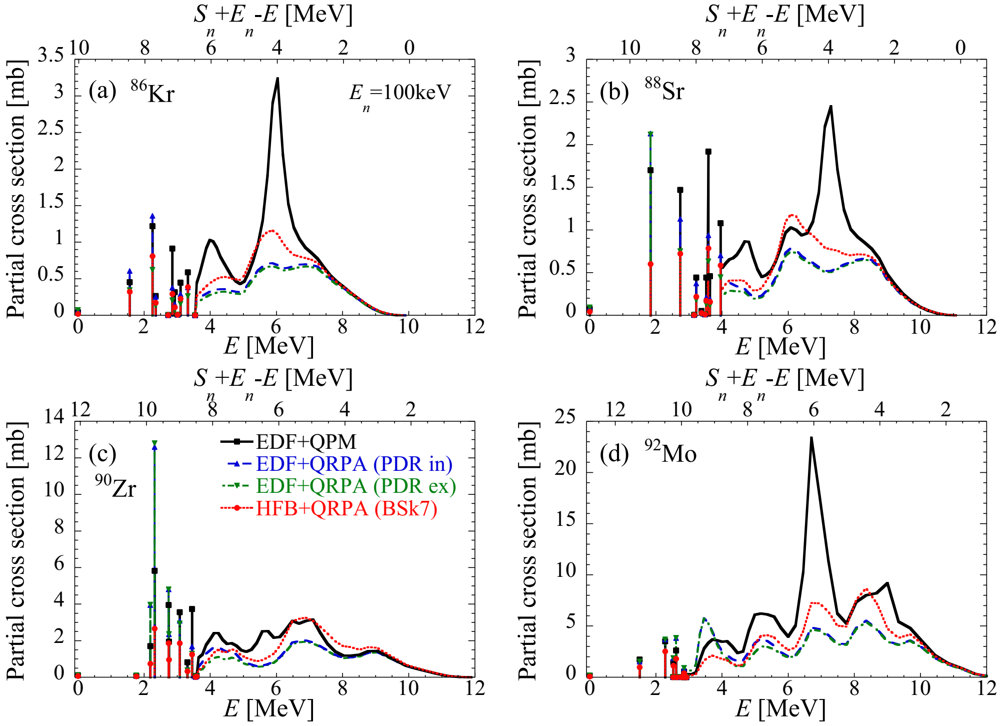

FIG. 4. (Color online) Partial (n,γ) cross sections to a CN state of energy E for incident neutrons (at an energy $E_n = 100$ keV) on (a) ^{85}Kr, (b) ^{87}Sr, (c) ^{89}Zr, and (d) ^{91}Mo calculated with TALYS using EDF plus three-phonon QPM (black solid line), EDF + QRPA (PDR included) (blue dashed line), EDF + QRPA (PDR excluded) (green dash-dotted line), and HFB + QRPA (BSk7) (red dotted line) strength functions. E corresponds to the excited states in the CN, either described by discrete known levels or above the last known level by the HFB plus combinatorial NLD [53]. The upper x axis corresponds to the emitted γ-ray energy $E_\gamma = S_n + E_n - E$.

TABLE III. Maxwellian-averaged cross sections (in mb) at the thermal energy of $kT = 30$ keV obtained for the four reactions studied and the four strength functions, i.e., EDF + three-phonon QPM, EDF + QRPA (PDR included), EDF + QRPA (PDR excluded), and HFB + QRPA (BSk7). Experimental data are given when available. For the ^{85}Kr$(n,\gamma)^{86}$Kr reaction, the experimental value correspond to the Maxwellian-averaged cross section determined with the experimental strength as derived in Ref. [5].

	Exp.	EDF + QPM	EDF + QRPA (PDR in)	EDF + QRPA (PDR ex)	HFB + QRPA (BSk7)
^{85}Kr$(n,\gamma)^{86}$Kr	83^{+23}_{-38} [5]	104.0	53.1	37.3	59.0
^{87}Sr$(n,\gamma)^{88}$Sr	92 ± 4 [7]	103.1	54.2	44.4	62.1
^{89}Zr$(n,\gamma)^{90}$Zr	–	224.3	170.4	152.1	159.8
^{91}Mo$(n,\gamma)^{92}$Mo	–	349.8	174.8	158.4	195.0

systematically larger than the QRPA one (see Fig. 1), except for ^{90}Zr. This explains the differences in the neutron-capture cross sections observed in Fig. 3. Similarly, the strong 9–10-MeV dipole strength enhancement obtained within the QRPA models is reflected in the large partial cross section to the first excited states of energy $E_x \simeq 2$ MeV (which are populated by $E1$ deexcitations from the compound states produced by s- and p-wave neutron captures on the $9/2^+$ ground state).

The various Maxwellian-averaged cross sections at the thermal energy of $kT = 30$ keV are summarized in Table III and seen to reflect the same tendency as the one observed in Fig. 3. The EDF + QPM model with its enhanced low-lying strength gives rise to cross sections significantly larger than the ones predicted by the QRPA model and in good agreement with available experimental data. By comparison of the results obtained by EDF + QRPA (PDR in) and EDF + QRPA (PDR ex) dipole strength functions, the contribution of the pure PDR to the Maxwellian-averaged cross sections is estimated to be of the order of ~30% for ^{85}Kr$(n,\gamma)^{86}$Kr, ~20% for ^{87}Sr$(n,\gamma)^{88}$Sr, ~11% for ^{89}Zr$(n,\gamma)^{90}$Zr, and ~9% for ^{91}Mo$(n,\gamma)^{92}$Mo, as shown in Table III. The smooth decrease of the reaction cross sections could be connected to the decreasing N/Z ratio toward ^{92}Mo. Note that at 30 keV, the contribution from thermally populated excited states in the target nucleus is negligible for the four reactions considered here.

As a possible application of astrophysical interest, we show in Fig. 5 the predicted ^{89}Zr$(n,\gamma)^{90}$Zr and ^{91}Mo$(n,\gamma)^{92}$M neutron-capture cross sections. Although such reactions do not enter any nucleosynthesis path as such, their reverse photoneutron emissions, traditionally obtained from detailed balance relations from the radiative capture, correspond to the possible destruction of $N = 50$ isotones during the p-process nucleosynthesis [12]. To estimate the corresponding radiative neutron-capture cross section, we adopt the three-phonon QPM $E1$ strength, which as been shown to reproduce experimental strengths (Fig. 1) and cross sections (Fig. 3) rather well. However, as discussed in Sec. III, NLD may also affect significantly (n,γ) cross sections. For this reason, we have considered here five different NLD models [49,53,54] to estimate the possible uncertainty range in the predictions, as shown in Fig. 5. Note that for the present cases NLD are normalized to reproduce the cumulative number of low-lying states (see [49] for more details on the normalization), but no experimental s-wave spacings at the neutron threshold exist, so that rather large uncertainties still affect NLD predictions and hence radiative neutron-capture cross sections.

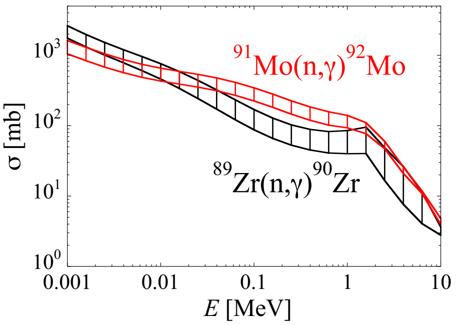

FIG. 5. (Color online) Neutron-capture cross sections of ^{89}Zr$(n,\gamma)^{90}$Zr and ^{91}Mo$(n,\gamma)^{92}$Mo calculated with TALYS using the three-phonon QPM strength function and five different NLD models from Refs. [49,53,54].

C. Proton captures

To test the newly derived strength functions in $N = 50$ nuclei, it is also of particular interest to study the radiative proton-capture reaction ^{89}Y$(p,\gamma)^{90}$Zr recently remeasured in Ref. [62]. In this case, the cross section becomes sensitive to the γ-ray strength function essentially above the neutron emission threshold around 3.6 MeV. Below this threshold, the cross section is only sensitive to the proton-nucleus optical

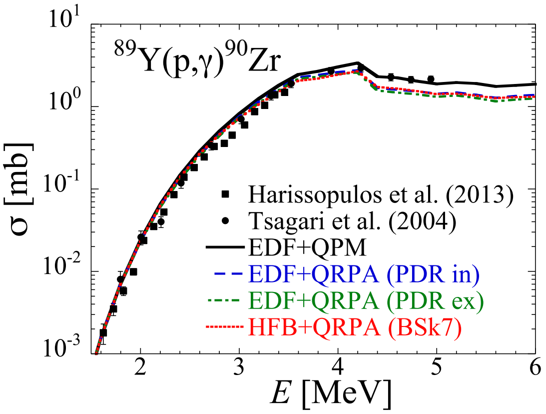

FIG. 6. (Color online) Radiative proton-capture cross section ^{89}Y$(p,\gamma)^{90}$Zr calculated with TALYS using EDF plus three-phonon QPM (black solid line), EDF + QRPA (PDR included) (blue dashed line), EDF + QRPA (PDR excluded) (green dash-dotted line), and HFB + QRPA (BSk7) (red dotted line) strength functions. Experimental data from [62,63].

potential [44]. As shown in Fig. 6, the QPM model allows for a significantly better description of the cross section above 4 MeV, at least for the adopted HFB plus combinatorial NLD model [53]. The QRPA models lead to a rather underestimation of the cross section and the PDR contribution is found to have a rather small impact of no more than 5% to 10%.

V. CONCLUSIONS

In conclusion, the contribution of the PDR to radiative capture cross sections for 10–100-keV incident neutrons is systematically investigated in $N = 50$ isotones. The results obtained with EDF + QRPA calculations indicate that they are correlated with the neutron skin thickness. Thus, the largest PDR impact, of the order of ~50%, is observed for the ^{85}Kr$(n,\gamma)^{86}$Kr reaction, where the target nucleus ^{85}Kr has the largest $N/Z = 1.43$ ratio in comparison with the other nuclei considered. The effect smoothly decreases with the decrease of the N/Z ratio towards ^{91}Mo ($N/Z = 1.22$) and its contribution to the ^{91}Mo$(n,\gamma)^{92}$Mo reaction cross section is of the order of 10%. Similar results are also found in the examination of Maxwellian-averaged cross sections at the thermal energy of $kT = 30$ keV. Accordingly, with decreasing N/Z ratio the Maxwellian-averaged cross sections also decrease from of about 30% for the ^{85}Kr$(n,\gamma)^{86}$Kr reaction to of about 9% for the ^{91}Mo$(n,\gamma)^{92}$Mo reaction.

The PDR contribution to the radiative proton-capture cross section for the ^{89}Y$(p,\gamma)^{90}$Zr reaction is found to be small, less than ~10%.

In these studies, a common observation is that the QRPA is not sufficient to describe the nuclear excitations below the neutron threshold; hence, the radiative capture cross sections at astrophysical energies. The systematic comparison between EDF + QRPA and the three-phonon QPM calculations in $N = 50$ nuclei shows that the behavior of the low-energy dipole strength is influenced by the competition between static and dynamical effects. The first one is related to the mean field and the pure PDR associated with neutron skin oscillations, while the second one represents the coupling of the single-particle states with a complex core polarization. The latter leads to the redistribution and fragmentation of the electric dipole strength.

Consequently, our three-phonon QPM investigations indicate that the radiative capture cross section is underestimated by a factor of about two by the QRPA in all considered cases [except for the ^{89}Zr$(n,\gamma)^{90}$Zr reaction, where this factor is slightly smaller]. The good agreement achieved between theory and experimental data, where available, confirms the importance of the multiphonon coupling and the relevance of the three-phonon QPM for astrophysical applications. Of particular significance is the demonstrated ability of the involved theoretical method for predictions and exploratory investigations of radiative capture cross sections in hitherto experimentally inaccessible mass regions.

ACKNOWLEDGMENTS

The work is supported by BMBF Grant No.05P12RGFTE. S.G. acknowledges support from the FRS-FNRS.

[1] E. M. Burbidge *et al.*, Rev. Mod. Phys. **29**, 547 (1957).
[2] B. S. Meyer, Annu. Rev. Astron. Astrophys. **32**, 153 (1994).
[3] M. Arnould and K. Takahashi, Rep. Prog. Phys. **62**, 395 (1999).
[4] F. Käppeler, Prog. Part. Nucl. Phys. **43**, 419 (1999).
[5] R. Raut, A. P. Tonchev, G. Rusev, W. Tornow, C. Iliadis, M. Lugaro, J. Buntain, S. Goriely, J. H. Kelley, R. Schwengner, A. Banu, and N. Tsoneva, Phys. Rev. Lett. **111**, 112501 (2013).
[6] V. G. Soloviev, *Theory of Complex Nuclei* (Pergamon, Oxford, 1976).
[7] Z. Y. Bao, H. Beer, F. Käppeler, F. Voss, K. Wisshak, and T. Rauscher, At. Data Nucl. Data Tables **76**, 70 (2000).
[8] M. Arnould, S. Goriely, and K. Takahashi, Phys. Rep. **450**, 97 (2007).
[9] A. J. Koning and D. Rochman, Nucl. Data Sheets **113**, 2841 (2012), and references therein.
[10] Y. Xu, S. Goriely, A. J. Koning, and S. Hilaire, Phys. Rev. C **90**, 024604 (2014), and references therein.
[11] S. Goriely, Phys. Lett. B **436**, 10 (1998).
[12] M. Arnould and S. Goriely, Phys. Rep. **384**, 1 (2003).
[13] D. Savran, T. Aumann, and A. Zilges, Prog. Part. Nucl. Phys. **70**, 210 (2013), and references therein.
[14] B. L. Berman, At. Data Nucl. Data Tables **15**, 319 (1975).
[15] R. Schwengner, G. Rusev, N. Tsoneva, N. Benouaret, R. Beyer, M. Erhard, E. Grosse, A. R. Junghans, J. Klug, K. Kosev, H. Lenske, C. Nair, K. D. Schilling, and A. Wagner, Phys. Rev. C **78**, 064314 (2008).
[16] R. Schwengner, R. Massarczyk, G. Rusev, N. Tsoneva, D. Bemmerer, R. Beyer, R. Hannaske, A. R. Junghans, J. H. Kelley, E. Kwan, H. Lenske, M. Marta, R. Raut, K. D. Schilling, A. Tonchev, W. Tornow, and A. Wagner, Phys. Rev. C **87**, 024306 (2013).
[17] P. Van Isacker, M. A. Nagarajan, and D. D. Warner, Phys. Rev. C **45**, R13 (1992).
[18] N. Tsoneva and H. Lenske, Phys. Rev. C **77**, 024321 (2008), and references therein.
[19] S. Volz, N. Tsoneva, M. Babilon, M. Elvers, J. Hasper, R.-D. Herzberg, H. Lenske, K. Lindenberg, D. Savran, and A. Zilges, Nucl. Phys. A **779**, 1 (2006).
[20] N. Tsoneva, H. Lenske, and Ch. Stoyanov, Phys. Lett. B **586**, 213 (2004).
[21] P. Ring and P. Schuck, *The Nuclear Many-Body Problem* (Springer Verlag, Berlin, 2004).
[22] M. Grinberg and Ch. Stoyanov, Nucl. Phys. A **573**, 231 (1994).
[23] A. Avdeenkov, S. Goriely, S. Kamerdzhiev, and S. Krewald, Phys. Rev. C **83**, 064316 (2011).
[24] B. Özel-Tashenov *et al.*, Phys. Rev. C **90**, 024304 (2014).
[25] E. Litvinova, H. P. Loens, K. Langanke, G. Martínez-Pinedo, T. Rauscher, P. Ring, F.-K. Thielemann, and V. Tselyaev, Nucl. Phys. A **823**, 26 (2009).
[26] F. Knapp, N. Lo Iudice, P. Vesely, F. Andreozzi, G. De Gregorio, and A. Porrino, Phys. Rev. C **90**, 014310 (2014).
[27] S. Goriely and E. Khan, Nucl. Phys. A **706**, 217 (2002).
[28] S. Goriely, E. Khan, and M. Samyn, Nucl. Phys. A **739**, 331 (2004).
[29] I. Daoutidis and S. Goriely, Phys. Rev. C **86**, 034328 (2012).

[30] E. Khan, N. Sandulescu, M. Grasso, and N. V. Giai, Phys. Rev. C **66**, 024309 (2002).

[31] A. P. Tonchev, S. L. Hammond, J. H. Kelley, E. Kwan, H. Lenske, G. Rusev, W. Tornow, and N. Tsoneva, Phys. Rev. Lett. **104**, 072501 (2010).

[32] G. Rusev, N. Tsoneva, F. Dönau, S. Frauendorf, R. Schwengner, A. P. Tonchev, A. S. Adekola, S. L. Hammond, J. H. Kelley, E. Kwan, H. Lenske, W. Tornow, and A. Wagner, Phys. Rev. Lett. **110**, 022503 (2013).

[33] F. Hofmann and H. Lenske, Phys. Rev. C **57**, 2281 (1998).

[34] P. Hohenberg and W. Kohn, Phys. Rev. **136**, B864 (1964).

[35] W. Kohn and L. J. Sham, Phys. Rev. **140**, A1133 (1965).

[36] G. Audi, M. Wang, A. H. Wapstra, F. G. Kondev, M. MacCormick, X. Xu, and B. Pfeiffer, Chin. Phys. C **36**, 1287 (2012).

[37] N. Tsoneva and H. Lenske, Phys. Lett. B **695**, 174 (2011).

[38] A. I. Vdovin and V. G. Soloviev, Sov. J. Part. Nucl. **14**, 237 (1983).

[39] V. Yu. Ponomarev, Ch. Stoyanov, N. Tsoneva, and M. Grinberg, Nucl. Phys. A **635**, 470 (1998).

[40] R. Capote *et al.*, Nucl. Data Sheets **110**, 3107 (2009).

[41] M. Beard, S. Frauendorf, B. Kämpfer, R. Schwengner, and M. Wiescher, Phys. Rev. C **85**, 065808 (2012).

[42] D. M. Brink, Ph.D. thesis, Oxford University, 1955.

[43] S. Goriely and J. P. Delaroche, Phys. Lett. B **653**, 178 (2007).

[44] A. J. Koning and J. P. Delaroche, Nucl. Phys. A **713**, 231 (2003).

[45] T. Belgya, O. Bersillon, R. Capote, T. Fukahori, G. Zhigang, S. Goriely, M. Herman, A. V. Ignatyuk, S. Kailas, A. Koning, P. Obložinský, V. Plujko, and P. Young, *Handbook for Calculations of Nuclear Reaction Data, RIPL-2* (IAEA, Vienna, 2006), IAEA-TECDOC-1506, http://www-nds.iaea.org/RIPL-2/

[46] A. Gilbert and A. G. W. Cameron, Can. J. Phys. **43**, 1446 (1965).

[47] J. R. Huizenga and L. G. Moretto, Ann. Rev. Nucl. Sci. **22**, 427 (1972).

[48] A. V. Ignatyuk, IAEA Report, TECDOC-1034, 1998.

[49] A. J. Koning, S. Hilaire, and S. Goriely, Nucl. Phys. A **810**, 13 (2008).

[50] P. Decowski *et al.*, Nucl. Phys. A **110**, 129 (1968).

[51] L. G. Moretto, Nucl. Phys. A **185**, 145 (1972).

[52] M. Hillman and J. R. Grover, Phys. Rev. **185**, 1303 (1969).

[53] S. Goriely, S. Hilaire, and A. J. Koning, Phys. Rev. C **78**, 064307 (2008).

[54] S. Hilaire, M. Girod, S. Goriely, and A. J. Koning, Phys. Rev. C **86**, 064317 (2012).

[55] J. B. French and K. F. Ratcliff, Phys. Rev. C **3**, 94 (1971).

[56] N. Cerf, Phys. Rev. C **50**, 836 (1994).

[57] H. Nakada and Y. Alhassid, Phys. Rev. Lett. **79**, 2939 (1997).

[58] Y. Alhassid, S. Liu, and H. Nakada, Phys. Rev. Lett. **83**, 4265 (1999).

[59] S. Goriely, M. Samyn, M. Bender, and J. M. Pearson, Phys. Rev. C **68**, 054325 (2003).

[60] G. Walter, Kernforschungszentrum Karlsruhe Reports No. 3706, 1984.

[61] R. L. Macklin and J. H. Gibbons, Phys. Rev. **159**, 1007 (1967).

[62] S. Harissopulos, A. Spyrou, A. Lagoyannis, M. Axiotis, P. Demetriou, J. W. Hammer, R. Kunz, and H. W. Becker, Phys. Rev. C **87**, 025806 (2013).

[63] P. Tsagari, M. Kokkoris, E. Skreti, A. G. Karydas, S. Harissopulos, T. Paradellis, and P. Demetriou, Phys. Rev. C **70**, 015802 (2004).